Electronic Supplementary Material (ESI) for J. Mater. Chem. C.

Supporting information

Near-infrared Organic Photodetector Based on An Aza-BODIPY Dye for Laser Microphone System

Xi Chen,[1,a] Bo Yu,[1,a] Jiawei Wang,[a] Zhongzhong Luo,[b] Haixing Meng,[a] Boming Xie,[b] Ruyi Zhou,[a] Shujuan Liu,*[,a] and Qiang Zhao*[,a,b]

a. State Key Laboratory of Organic Electronics and Information Displays and Jiangsu Key Laboratory for Biosensors, Institute of Advanced Materials (IAM) & Institute of Flexible Electronics (Future Technology), Nanjing University of Posts and Telecommunications, 9 Wenyuan Road, Nanjing, Jiangsu 210023, P. R. China; E-mail: iamsjliu@njupt.edu.cn, iamqzhao@njupt.edu.cn.

b. College of Electronic and Optical Engineering & College of Flexible Electronics (Future Technology), Jiangsu Province Engineering Research Center for Fabrication and Application of Special Optical Fiber Materials and Devices, Nanjing University of Posts and Telecommunications, 9 Wenyuan Road, Nanjing, Jiangsu 210023, P. R. China.

Contents

Part I.

Materials preparation and characterization

All starting reagents and materials were purchased from commercial sources and used without further purification. BODIPY-F was synthesized according to the previously reported procedures[1,2]. Cyclic voltammetry (CV) was measured by a CHI660E electrochemical workstation in dry dichloromethane with a Pt disk, a Pt wire and an $Ag/AgNO_2$ were used as working, counter and reference electrodes respectively. Thermogravimetric analysis was obtained from NETZSCH STA-2500 regulus. The ^1H NMR spectra were recorded on a Bruker Ultra Shield Plus 400 MHz NMR instrument at 298 K using deuterated solvents. Chemical shifts were given in ppm, and were referenced against external Me_4Si (^1H).

Theoretical calculations of materials

Density functional theory (DFT) was used to optimize the ground-state structure of **BODIPY-F** under the B3LYP/6-31G(d) level, and vibrational frequency calculations were performed to verify the minimum nature of the optimized structures. Time-dependent density functional theory (TD-DFT) calculation was carried out to obtain the vertical excited states under B3LYP/6-31G(d) level based on the S_0 structure. The DFT/TDDFT calculations were performed on Gaussian 09 package.[3] Analysis and visualization of hole-electron distribution were finished by Multiwfn 3.8(dev) and VMD.[4]

Device Fabrication and Characterization

PEDOT:PSS film was chosen as the ideal hole injection layer (30 nm), which was formed by spin coating (3000 rpm for 30 s) of PEDOT:PSS solution on cleaned ITO substrates and followed by annealing at 120 °C for 30 min. Fully dissolve BODIPY-F and PCBM in 1,2-dichlorobenzene solvent (stir for 2 hours at 60 °C), and mix them with different weight ratios and stir for more than 12 hours to obtain BODIPY-F:PCBM precursor solution. BODIPY-F:PCBM precursor solution was spin coating (1000 rpm for 30 s) on the PEDOT:PSS-coated substrates and annealed at 120 °C for 10 minutes to obtain active layer films. C_{60} layer (10 nm) as electron transfer layer (ETL) and Al top electrode (100 nm) were subsequently deposited by thermal evaporation. The effective device area is defined by a shadow mask to be 4 mm^2. In addition, all experimental steps were carried out in a vacuum environment. DektakXTstep instrument is used to observe the film thickness. Atomic Force Microscopy (AFM, SPA 300 HV with a Bruker Nanoscope V, Brooke Technology, Germany) is used to test the surface roughness of films at roomtemperature and in air. UV-visible-NIR absorption spectra of the films on quartz substrates were recorded by using a Shimadzu UV-3600 spectrophotometer. The current density-voltage (*J-V*) characteristics of the NIR-OPD were collected by using a Keithley 4200A-SCS semiconductor parameter analyzer. The external quantum efficiency (*EQE*) of the devices was measured on Enlitech QER3018 by using calibrated Si and Ge diodes (Enli technology Co. Ltd.) as references.

Measurement of transient photocurrent speed and the laser microphone system

In order to observe the transient photocurrent speed of OPDs in NIR range, we prepared a metal probe to debase external effects due to week transmission of electrical signals (Figure S10). To reduce the impact of inductance rate of the entire circuit, the cable connecting the equipment and oscilloscope was connected to the fast Neill-Concelman connector. After the test circuit is built, the device area is irradiated with a modulated laser beam. In addition, the above experiment was carried out in an enclosed dark chamber. In the laser microphone system, the LM386 used in the optical communication circuit is a classic audio power amplifier, produced by Guangdong HGSEMi Corporation. In the LM386 operational amplifier circuit，pin 1 and pin 8 of the LM386 were the voltage gain setting port, $\text{gain value} = 30000/(150 + 1350 \times r/(1350 + r))$, where r is the resistance value of the resistor connected in series between pin 1 and pin 8. The voltage gain was set to 200 times by connecting a capacitor (C_1 = 10 μF) directly in series between pin 1 and pin 8. Then pin 3 connected the NIR-OPD and a variable resistor R_1 (0~10 kΩ), where the variable resistor R_1 was used to adjust the sound level from the speaker (R_2=10 Ω, C_2=250 μF, C_3=10 μF, C_4=0.05 μF). The capacitors and resistors used are produced by Taiwan YageoCorporation. The light density of the application part of the NIR laser diode is 50 mW/cm^2 and the distance between the light source and the photodetector is 0.5 m.

Part II. Synthetic procedures and characterizations.

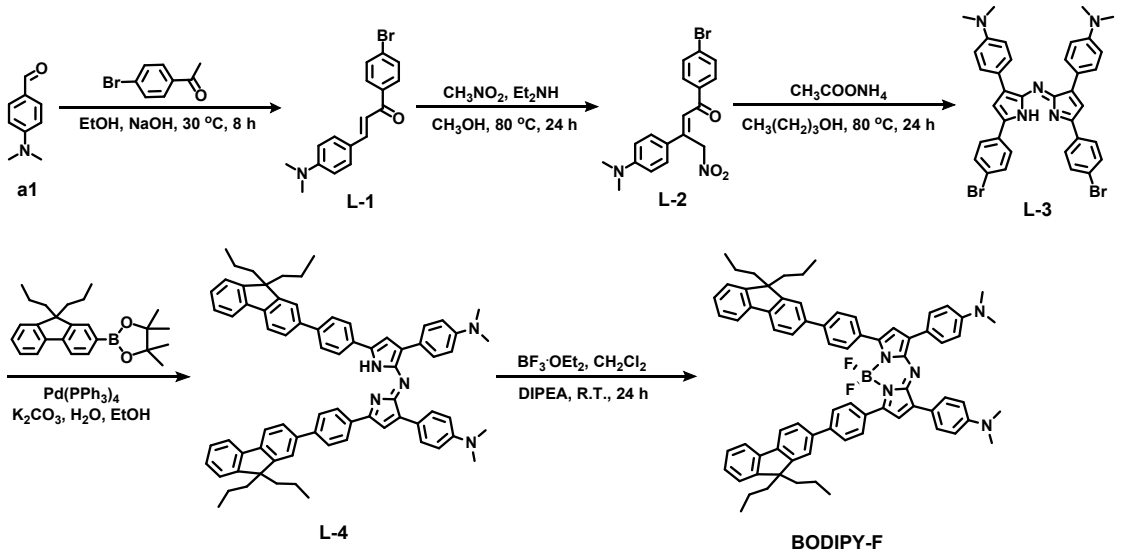

Scheme S1. Synthetic routes of BODIPY-F.

Synthesis of L-1. 1-(4-Bromophenyl) ethanone (1.49 g, 10.0 mmol), a1 (2.0 g, 10.0 mmol) and potassium hydroxide (40.0 mg, 1.0 mmol) were dissolved in ethanol/water (85:15 v/v, 200 mL) and stirred at room temperature for 24 h. During the course of the reaction, the product was precipitated from the reaction mixture. The reaction mixture was filtered and the resulting solid was washed with ethanol as a yellow solid (1.53 g, 93%). ^{1}H NMR (400 MHz, DMSO-d_6): δ = 8.03 (d, *J* = 7.2 Hz, 2H), 7.74-7.66 (m, 4H), 7.59(d, *J* = 15.2 Hz, 2H), 6.72 (d, *J* = 7.6 Hz, 2H), 2.99 (s, 6H).

Synthesis of L-2. Compound L-1 (1.32 g, 4 mmol), nitromethane (1.07 g, 0.02 mmol) anddiethylamine (1.46 g, 0.02 mmol) were dissolved in methanol (50 mL) and heated underreflux for 24 h. The reaction mixture was cooled to 0 ^{o}C. The mixture was acidified with 1 M HCl to pH = 3 and then extracted with dichloromethane/water. The organic solvent was evaporated under reduced pressure. The obtained crude product was recrystallized fromdichloromethane and methanol. Compound L-**2** was obtained as white solid (0.92 g, 64%). ^{1}H NMR (400 MHz, CDCl3): δ = 7.77 (d, *J* = 8.9 Hz, 2H), 7.59 (d, *J* = 8.4 Hz, 2H), 7.11 (d, *J* =8.8 Hz, 2H), 6.66 (d, *J* = 8.8 Hz, 2H), 4.78-4.73 (m, 1H), 4.65-4.60 (m, 1H), 4.13-4.06 (m,1H), 3.38 (m, 2H), 2.92 (s, 6H).

Synthesis of L-3. Compound L-2 (1.08 g, 2.8 mmol) and ammonium acetate (7.04 g, 91.4 mmol) in anhydrous butanol (100 mL) were heated under reflux for 24 h. The solution was cooled and the precipitate was filtered. The solid was washed with cold ethanol and isolated. The L-3 was obtained as blue solid (0.73 g, 67%). ^{1}H NMR (400 MHz, CDCl3): δ = 8.02 (d, *J* = 8.8 Hz, 4H), 7.76 (d, *J* = 8.8 Hz, 4H), 7.63 (d, *J* = 8.4 Hz, 4H), 7.01 (s, 2H), 6.78 (m, 5H), 3.05 (s, 12H).

Synthesis of L-4. A mixture of compound L-3 (346.0 mg, 0.5 mmol), **5** (300.0 mg, 1.05 mmol) and Pd (PPh3)4 (23.0 mg, 0.02 mmol) was first added to a round bottomed flask, and then a degassed mixture of toluene (2 mL), ethanol (1 mL) and aqueous 2 M potassium carbonate (1 mL) was injected under a nitrogen atmosphere. The mixture was stirred at 85 °C for 24 h. After cooling to room temperature, the mixture was washed with water and extracted with dichloromethane. The combined organic phase was concentrated and then purified by column chromatography on silica by using petroleum ether/dichloromethane (3:2) as eluent to obtain black solid (358.0 mg, 69%). ^{1}H NMR (400 MHz, CDCl3): δ = 8.11 - 8.06 (m, 8H), 7.86 (d, *J* = 7.8 Hz, 4H), 7.79 (d, *J* = 7.8 Hz, 2H), 7.74 (d, *J* = 7.2 Hz, 2H) , 7.70 (m, 4H), 7.40 - 7.31(m, 6H), 7.14 (s, 2H), 6.82 (d, *J* = 8.8 Hz, 4H), 3.07 (s, 12H), 2.04 (m, 8H), 0.70 (m, 20H); MALDI-TOF-MS (m/z): calcd for C74H73N5 1032.40; found 1031.49.

Synthesis of BODIPY-F. The anhydrous dichloromethane (20 mL) was used to dissolve the compound L-4 (103.0 mg, 0.1 mmol), and then the anhydrous disopropylethylamine (0.12 mL) was added into the mixture drop wise. And the BF3·Et2O (0.12 mL) was added to the mixture at 25 °C. Then, the mixture was stirred for 2 days. Dichloromethane (110 mL) and water (60 mL) were used to wash the crude product for 3 times. And the anhydrous Na2SO4 was used to dry the dichloromethane. To obtain the pure product, the column chromatographyon silica gel was utilized (1:2, dichloromethane: petroleum ether). Dark solid BODIPY-F (95.0mg, 87%) was obtained. ^{1}H NMR (400 MHz, CDCl3): δ = 8.19 (d, *J* = 8.4 Hz, 2H), 8.13 (d, *J* = 9.2 Hz, 2H) , 7.80 - 7.72 (m, 8H), 7.67 (m, 4H), 7.64 (m, 4H), 7.39 - 7.30 (m, 6H), 6.93 (s, 2H), 6.80 (d, *J* = 9.2 Hz, 4H), 3.07 (s, 12H), 2.00 (m, 8H), 0.69 (m, 20H) ppm; ^{19}F NMR

(376.5 MHz, $CDCl_3$): δ = -127.70 (q, 2F); MALDI-TOF-MS (m/z): calcd for C74H72BF2N5 1080.20; found 1079.67.

Part III. Supplementary table and figures

Table S1. DFT calculation of BODIPY-F

Compound	λ_{abs} (nm)	*f*	HOMO (eV)	LUMO (eV)
BODIPY-F	695	0.385	-4.89	-3.00

Table S2. Optical and electrochemical data of **BODIPY-F.**

Materials	$^{a}\lambda_{max}$ [nm]	$^{b}E_{1/2}^{Red}{}_{1}$ [V]	$^{b}E_{1/2}^{Ox}{}_{1}$ [V]	$^{b}E_{1/2}^{Ox}{}_{2}$ [V]	HOMO [eV]	LUMO [eV]	E_{gap} [eV]
BODIPY-F	676.5, 840	-0.68	0.49	0.65	-5.16	-3.88	1.28

[a.] Absorption spectra of BODIPY-F spin-coated on quartz plate. [b.] Calculated from the formula, $E_{HOMO} = -(E_{1/2}^{Ox1} - E(Fc/Fc^{+}) + 4.48)$; $E_{LUMO} = -(E_{1/2}^{Red1} - E(Fc/Fc^{+}) + 4.48)$ and $E(Fc/Fc^{+}) = 0.10$ V.

Table S3. Comparison of the OPD performance.

Device structure	R (A W^{-1})	D*(Jones)	Switching ratio	BW (kHz)/t_r (μs)	[Ref]
ITO/PEDOT:PSS/(PCE10:P3HT)/PCBM/LiF/Al	0.022 (780 nm)	1.2×10^{12}	2.3×10^{3} (-1.0 V)	3.5/-	[5]
ITO/PEDOT:PSS/ PNTT:PC71BM/Al	0.23 (760 nm)	3.37×10^{12}		20/-	[6]
ITO/ZnO/PTZBTTT-BDT:$PC_{71}BM$/MoO3/Ag	0.092 (640 nm)	1.71×10^{12}	2.2×10^{3} (-0.5 V)	-	[7]
ITO/PFNBr/PCE10:COTIC-4Cl: $PC_{71}BM$ /LiF/Al	0.35 (1050 nm)	5×10^{12}	-	1000/0.78	[8]
ITO/ZnO/PTB7-Th:ITIC/MoO_X/Ag/PEIE/PTB7-Th:FOIC/MoO_X/Ag	-	2.5×10^{11} (805 nm)	-	-/0.146	[9]
ITO/PEDOT:PSS/PMBBDT : N2200 /Au		4×10^{11}(860 nm)	-	-/600	[10]
ITO/PEDOT:PSS/PTB7-Th:COTIC-4F/PFN-Br/Al	0.4 (870 nm)	5.20×10^{11}		45/-	[11]
ITO/PEDOT:PSS/PM6:O4TFIC /Phen-NaDPO/Ag.	0.50 (890 nm)	9.00×10^{11}		38/	[12]
ITO/PEDOT:PSS/BODIPY-F:PCBM/C_{60}/Al	**0.125 (840 nm)**	**5.94×10^{11}**	**4.2×10^{3} (-0.5 V)**	**700/0.5**	**This work**

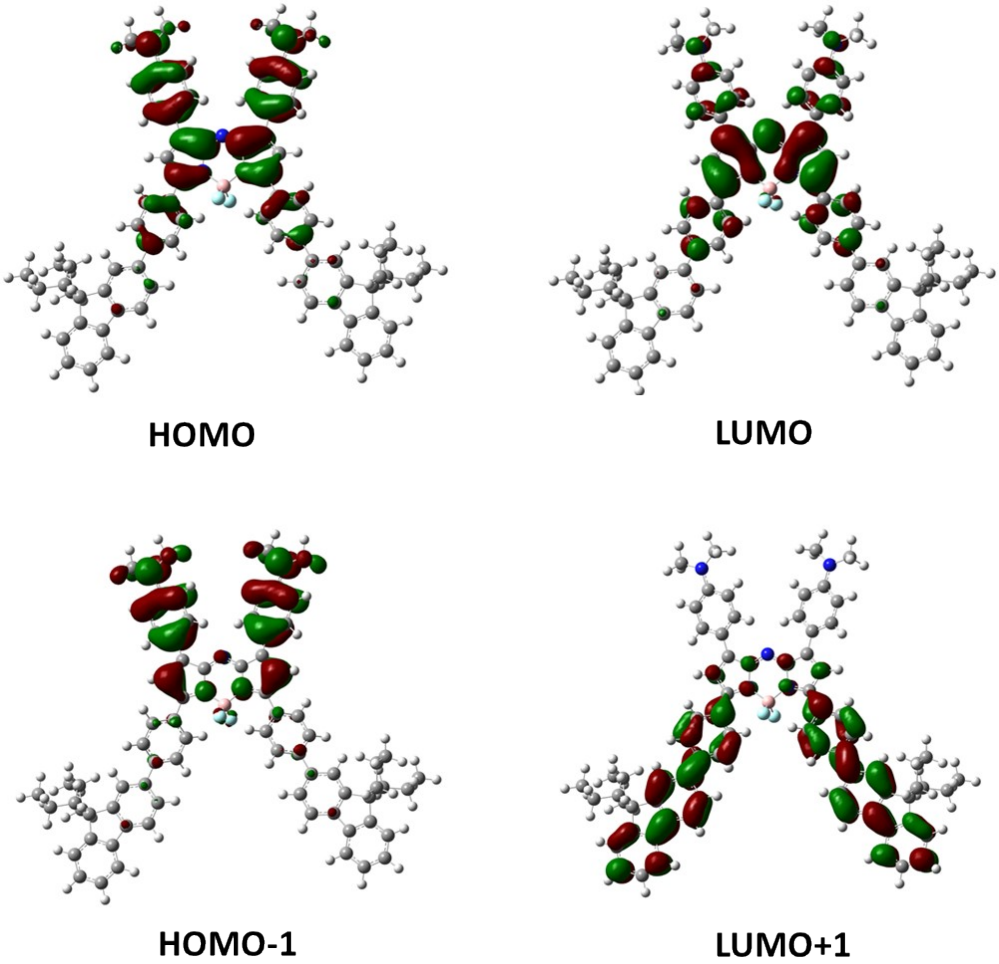

Figure S1. Orbital localization. Highest occupied orbitals (HOMO), HOMO-1, lowest unoccupied orbitals (LUMO) and LUMO+1 of molecules BODIPY-F calculated at the B3LYP/6-31G(d) level (Gaussian).

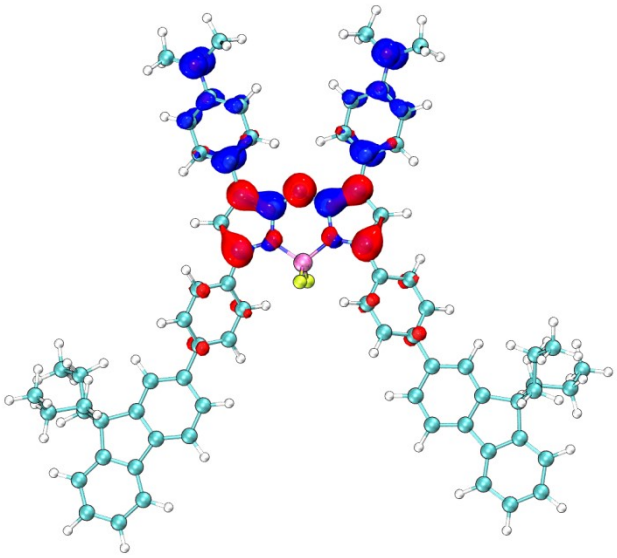

Figure S2. Calculated hole-electron distribution of $S_0 \rightarrow S_1$ (isovalue = 0.002) excitation in BODIPY-F. Blue and red regions represent the hole and electron distributions, respectively.

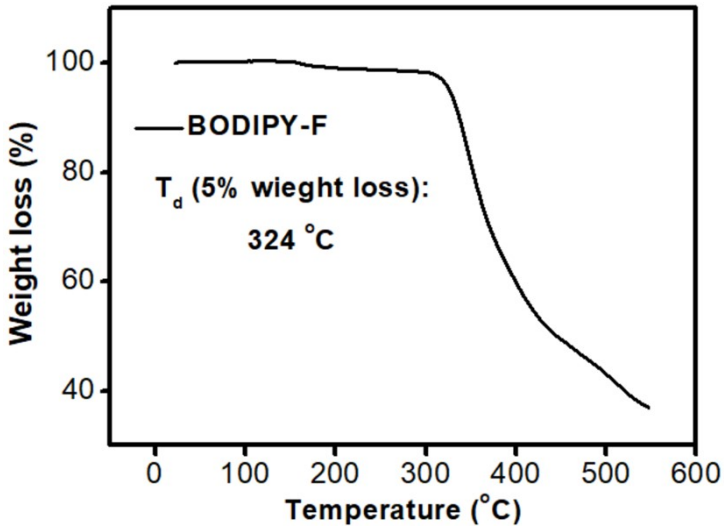

Figure S3. TGA traces of BODIPY-F under nitrogen atmosphere.

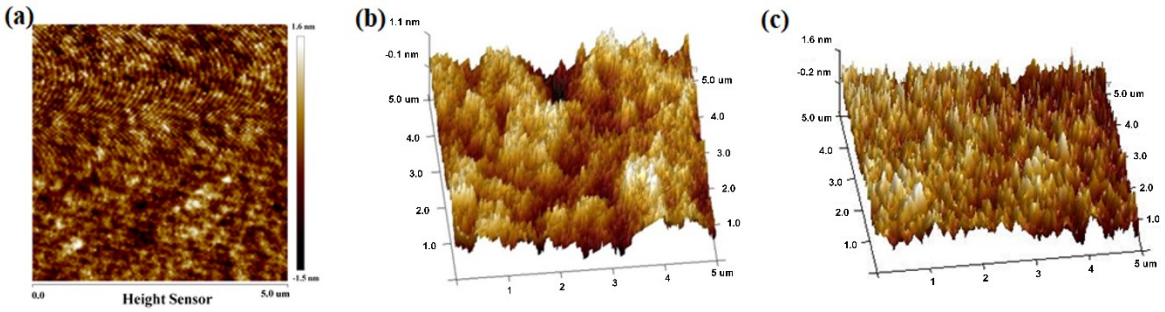

Figure S4. (a) 2D (BODIPY-F:PCBM = 0.2:1), (b) 3D (BODIPY-F:PCBM = 0.1:1) and (c) 3D (BODIPY-F:PCBM = 0.2:1) AFM height image of the active layer.

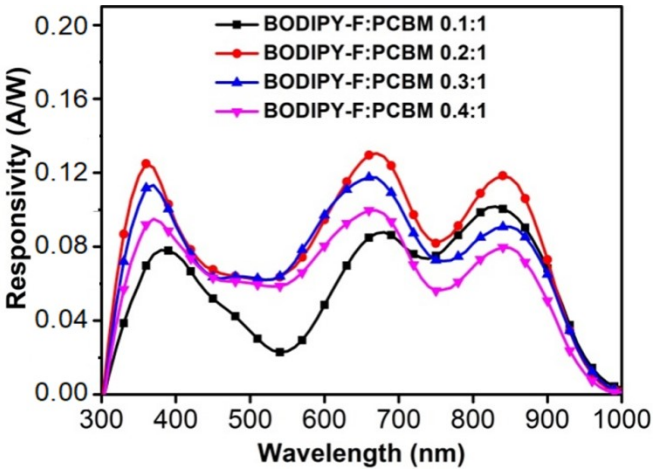

Figure S5. *R* of the NIR-OPDs with different doped ratio at bias of -5.0 V.

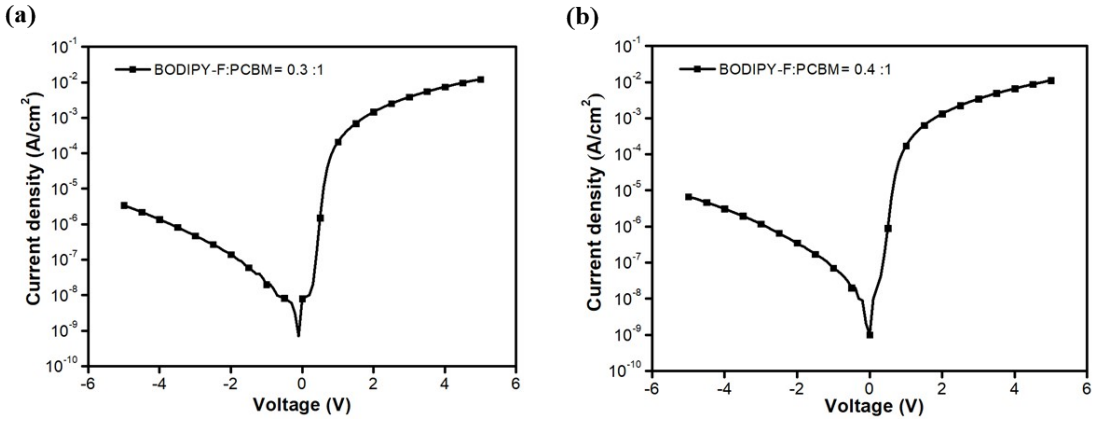

Figure S6. *J-V* curve of NIR-OPDs with various BODIPY-F:PCBM concentration ratios in the dark. (a) 0.3:1. (b) 0.4:1.

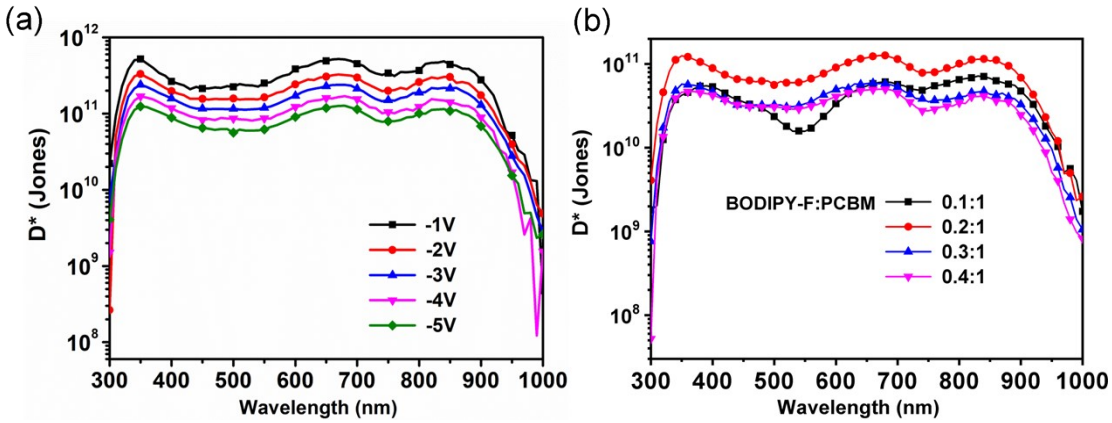

Figure S7. *D** curve of NIR-OPDs (a) based on BODIPY-F:PCBM (0.2:1) at different bias, (b) at bias of -5.0 V with different BODIPY-F:PCBM weight ratios.

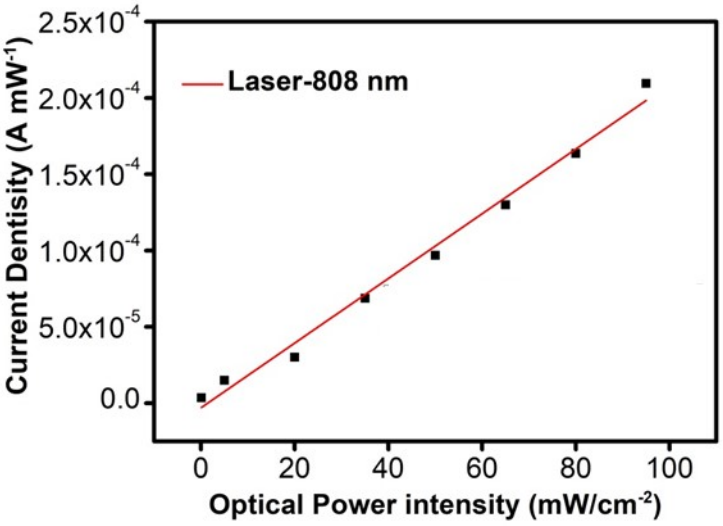

Figure S8. Photocurrent of NIR-OPD under the illumination of NIR laser with various intensities at -0.5 V bias.

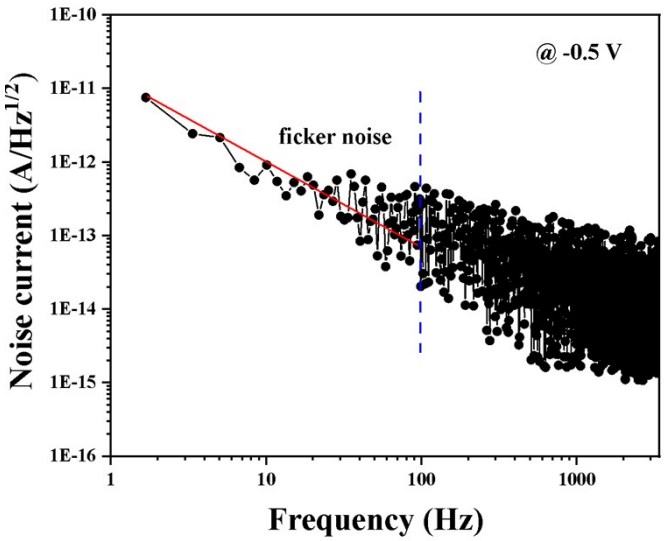

Figure S9. Noise density spectra of NIR-OPDs based on BODIPY-F:PCBM (0.2:1) at -0.5 V bias.

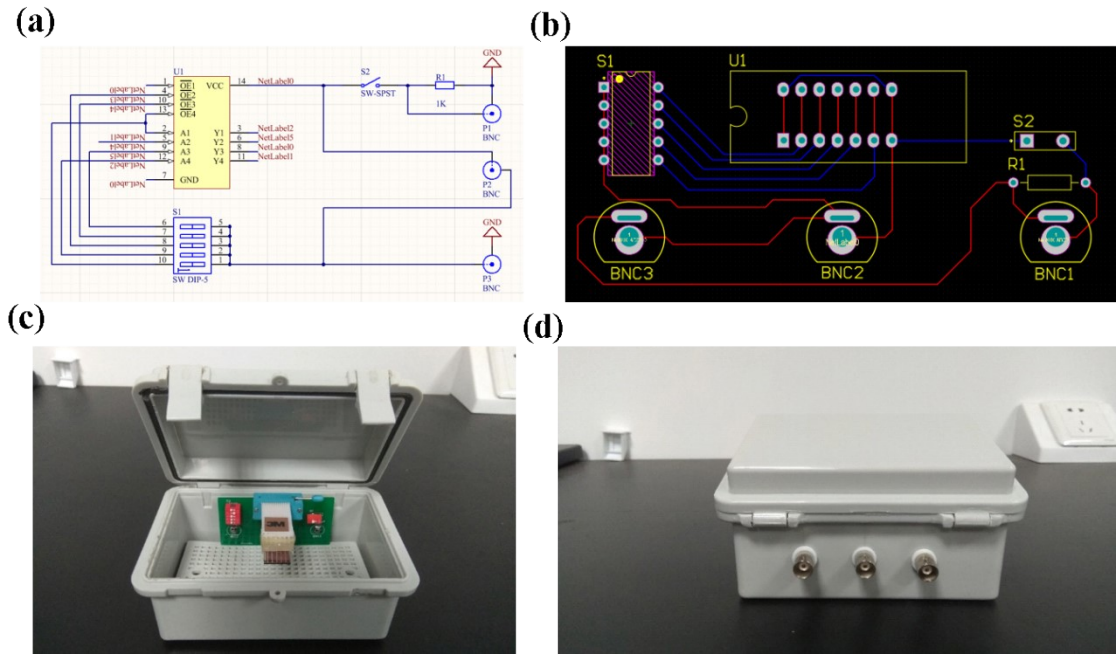

Figure S10. (a) Basic test circuit diagram schematic. (b) The circuit of PCB board (where red lines on the front of the PCB board, blue line on the back). (c) Front and (d) back of the test box.

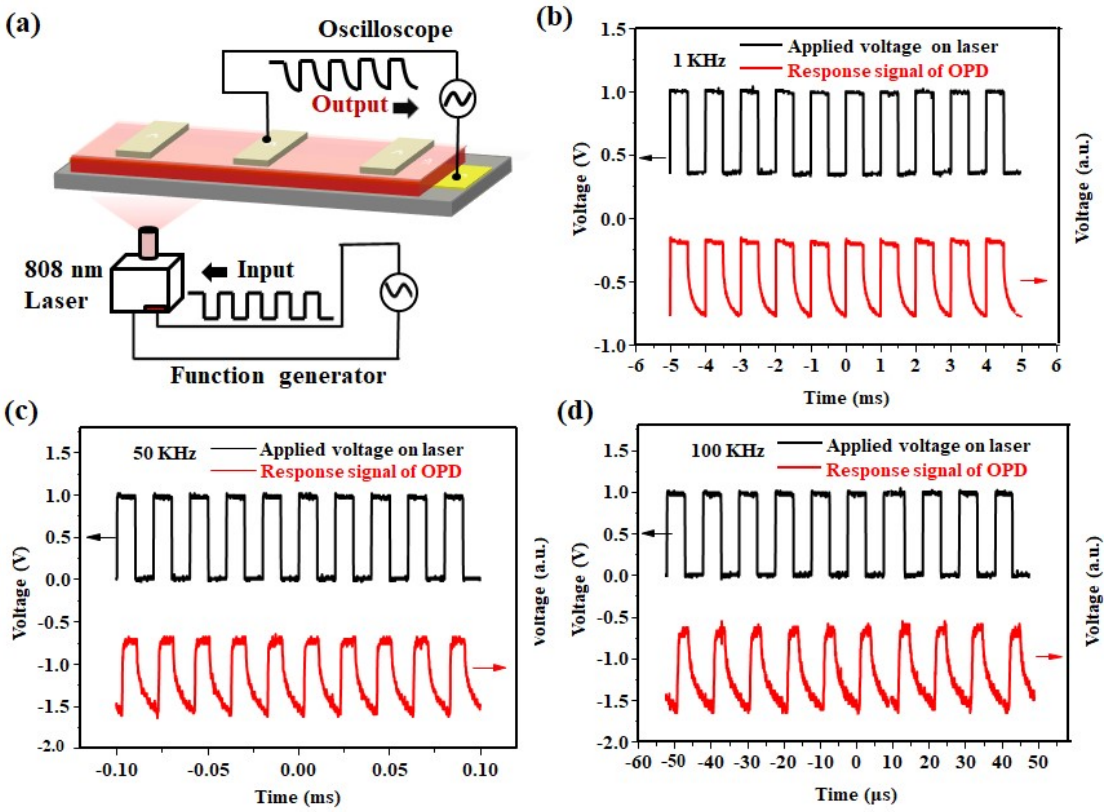

Figure S11. (a) Experimental setup to test transient photocurrent speed of the NIR light communication system. The input and output transient photocurrent signals of NIR light communication under the frequency of (b) 1 kHz, (c) 50 kHz and (d) 100 kHz.

Part IV. References.

1. M. Li, Y. Xu, M. Zhao, F. Li, W. Feng, T. Feng, S. Liu and Q. Zhao, *Inorg. Chem.,* 2020, **59**, 17826-17833.

2. G. Li, X. Zhang, W. Zhao, W. Zhao, F. Li, K. Xiao, Q. Yu, S. Liu and Q. Zhao, *ACS Appl. Mater. Interfaces,* 2020, **12**, 20180-20190.

3. G. W. T. M. J. Frisch, H. B. Schlegel, G. E. Scuseria, M. A. Robb, J. R. Cheeseman, G. Scalmani, V. Barone, B. Mennucci, G. A. Petersson, H. Nakatsuji, M. Caricato, X. Li, H. P. Hratchian, A. F. Izmaylov, J. Bloino, G. Zheng, J. L. Sonnenberg, M. Hada, M. Ehara, K. Toyota, R. Fukuda, J. Hasegawa, M. Ishida, T. Nakajima, Y. Honda, O. Kitao, H. Nakai, T. Vreven, J. A. Montgomery, Jr., J. E. Peralta, F. Ogliaro, M. Bearpark, J. J. Heyd, E. Brothers, K. N. Kudin, V. N. Staroverov, R. Kobayashi, J. Normand, K. Raghavachari, A. Rendell, J. C. Burant, S. S. Iyengar, J. Tomasi, M. Cossi, N. Rega, J. M. Millam, M. Klene, J. E. Knox, J. B. Cross, V. Bakken, C. Adamo, J. Jaramillo, R. Gomperts, R. E. Stratmann, O. Yazyev, A. J. Austin, R. Cammi, C. Pomelli, J. W. Ochterski, R. L. Martin, K. Morokuma, V. G. Zakrzewski, G. A. Voth, P. Salvador, J. J. Dannenberg, S. Dapprich, A. D. Daniels, Ö. Farkas, J. B. Foresman, J. V. Ortiz, J. Cioslowski, and D. J. Fox, *Gaussian **09***, Gaussian, Inc., Wallingford, CT 2009.

4. a) T. Lu, F. Chen, *J. Comput. Chem.* 2012, 33, 580; b) Z. Liu, T. Lu, Q. Chen, *Carbon* 2020, 165, 461; c) W. Humphrey, A. Dalke, K. Schulten, *J. Mol. Graph.,* 1996, **14**, 33.

5. J. Kim, S. Yoon, K. M. Sim and D. S. Chung, *J. Mater. Chem. C,* 2019, **7**, 4770-4777.

6**.** Z. Zeng, Z. Zhong, W. Zhong, J. Zhang, L. Ying, G. Yu, F. Huang and Y. Cao, *J. Mater. Chem. C,* 2019, **7**, 6070-6076.

7. X. Hu, K. Wang, C. Liu, T. Meng, Y. Dong, S. Liu, F. Huang, X. Gong and Y. Cao, *J. Mater. Chem. C,* 2014, **2**, 9592-9598.

8. Z. Zhong, F. Peng, L. Ying, G. Yu, F. Huang and Y. Cao, *Sci. China Mater.,* 2021, **64**, 2430-2438.

9. J. Liu, J. Jiang, S. Wang, T. Li, X. Jing, Y. Liu, Y. Wang, H. Wen, M. Yao, X. Zhan and L. Shen, *Small,* 2021, **17**, e2101316.

10. Z. Zhao, B. Liu, C. Xu, M. Liu, K. Yang, X. Zhang, Y. Xu, J. Zhang, W. Li and F. Zhang, *J. Mater. Chem. C,* 2021, **9**, 5349-5355.

11. C. Xu, P. Liu, C. Feng, Z. He and Y. Cao, *J. Mater. Chem. C,* 2022, **10**, 5787-5796.

12. M. Babics, H. Bristow, W. Zhang, A. Wadsworth, M. Neophytou, N. Gasparini and I. McCulloch, *J. Mater. Chem. C,* 2021, **9**, 2375-2380.